J. Opt. A: Pure Appl. Opt. **11** (2009) 125002 (8pp) doi:10.1088/1464-4258/11/12/125002

Size effects in the structural phase transition of VO_2 nanoparticles studied by surface-enhanced Raman scattering

E U Donev[1,3], J I Ziegler[1], R F Haglund Jr[1] and L C Feldman[1,2]

[1] Department of Physics and Astronomy, and Vanderbilt Institute of Nanoscale Science and Engineering, Vanderbilt University, Nashville, TN 37235, USA
[2] Institute for Advanced Materials, Devices and Nanotechnology, Rutgers, State University of New Jersey, Piscataway, NJ 08854, USA

E-mail: eugene@alumni.vanderbilt.edu

Received 6 July 2009, accepted for publication 10 August 2009
Published 21 September 2009
Online at stacks.iop.org/JOptA/11/125002

Abstract
We report the first experimental application of surface-enhanced Raman scattering (SERS) to the study of the structural phase transition of vanadium dioxide (VO_2). Using arrays of gold-capped VO_2 nanoparticles (Au + VO_2 NPs) and a VO_2 film covered with Au islands, we obtained the temperature evolution of the SERS intensity with respect to the amount of accessible material across the monoclinic–tetragonal–monoclinic transformation cycle of VO_2. The smallest Au + VO_2 NPs displayed the largest deviations from the bulk transition temperatures to complete the transformation, resulting in the widest thermal hysteresis, while the Au + VO_2 film exhibited the narrowest hysteresis. The observed size dependence agrees qualitatively with the model of defect-induced nucleation of the VO_2 transition, although the magnitude of the hysteresis width and its dependence on NP size were less pronounced than those in a previous study of elastic light scattering from bare VO_2 NPs. The discrepancies may stem from the creation of extrinsic nucleation sites in the VO_2 NPs during their high-temperature processing in the presence of the Au caps; alternatively, the hystereses of the structural and electronic transitions could each have a different dependence on size. Lastly, we correlate the size dependence of the VO_2 SERS intensity with the scattering efficiency of the Au nanoparticles, within the framework of a modified Mie-theory calculation.

Keywords: surface-enhanced Raman scattering (SERS), phase transition, hysteresis, size effects, Mie theory, vanadium dioxide (VO_2), gold (Au), hybrid nanoparticles, Au–VO_2

(Some figures in this article are in colour only in the electronic version)

1. Introduction

1.1. Motivation

Vanadium dioxide undergoes a much-studied phase transition at a nominal critical temperature $T_c \approx 340$ K in the bulk. Changes occur not only in the electronic configuration, but also in the crystallographic structure of the material, which switches from a monoclinic semiconductor below T_c to a tetragonal (rutile) metal above T_c [1–3]. The first-order nature of the transition results in a thermal hysteresis, whereby the material typically transforms at $T > T_c$ during heating and at $T < T_c$ during cooling. The fundamental driving mechanisms for the VO_2 phase transition have been discussed extensively for decades, and the debate regarding the relative roles of lattice distortion and electron–electron correlation continues to the present [4–14].

Interest in size effects in the VO_2 transition is relatively recent. Lopez *et al* studied ordered arrays of VO_2 NPs by incoherent elastic light scattering and reported size dependence

[3] Present address: Department of Electrical and Computer Engineering, University of Kentucky, Lexington, KY 40506, USA.

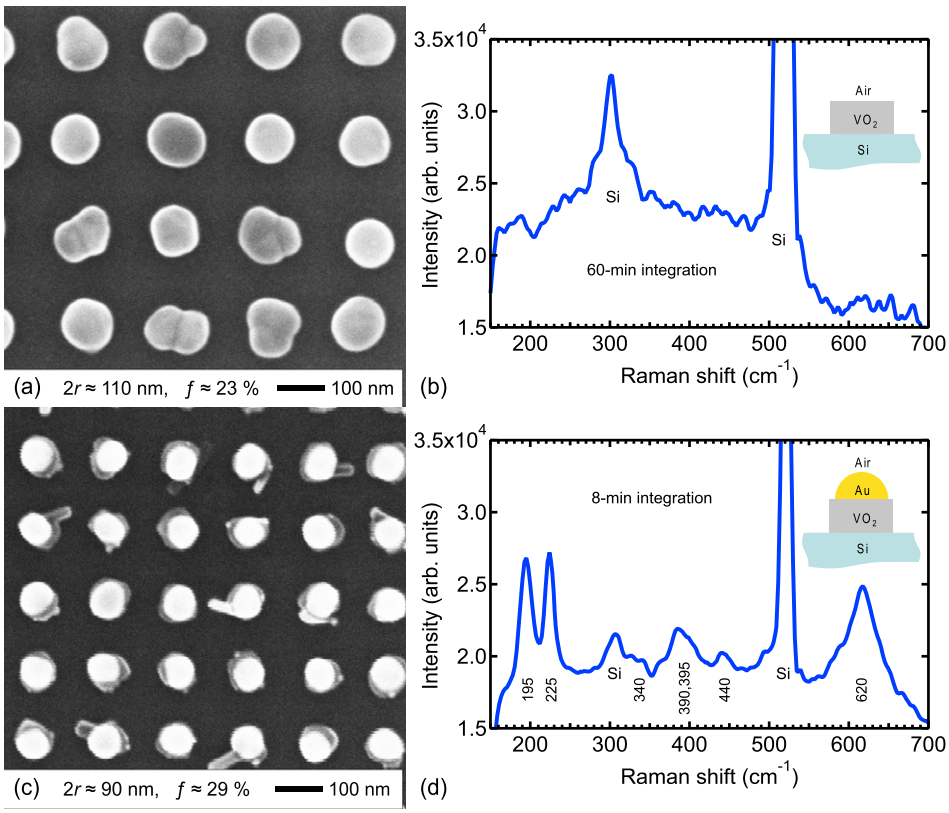

Figure 1. SEM images ($2r \equiv VO_2$ NP diameter; $f \equiv VO_2$ areal coverage) and room-temperature Raman spectra from arrays of ((a), (b)) bare and ((c), (d)) Au-capped VO_2 NPs on Si. Note the presence of several strong VO_2 peaks in the Au + VO_2 case, owing to signal enhancement (SERS effect) from the Au caps despite shorter collection time (8 versus 60 min) and smaller NP sizes (90 versus 110 nm).

as well as intrinsic variability in the transition temperatures of nominally identical NPs within the same array [15]. Hysteresis loops were observed to widen as the NP diameters decrease, in qualitative agreement with a model of defect-initiated nucleation of the VO_2 transition [16]. Since that light-scattering study [15] probed only the electronic response of VO_2 NPs, the present experiments were partly motivated by the desire to see whether a structural probe, such as the Raman-active phonon modes of the material, would yield a different size dependence and shed light on the structural characteristics of the VO_2 phase transition.

The present work was also motivated in part by a recently published Raman study of *single* VO_2 NPs of ∼150 nm diameter, where we demonstrated the feasibility of measuring a well-known signature of the structural transition of VO_2—the disappearance of certain Raman-active vibrational modes—in isolated nanoscale volumes of VO_2, and also recorded a hysteresis width of more than 55 K [17]. Such single-NP measurements provide a practical method for gathering particle-by-particle statistics on the defect sites responsible for nucleating the VO_2 transition. Therefore, as an intermediate step along this route, we set out to investigate the size-dependent properties of *arrays* of VO_2 NPs across their temperature-driven structural transformations.

1.2. SERS from hybrid Au + V O$_2$ NPs

While in the single-NP study [17] we measured the Raman response of 150 nm particles, we were unable to detect a usable Raman signal from arrays of VO_2 NPs smaller than about 100 nm in diameter. A scanning electron micrograph (SEM) of one such array on a silicon (Si) substrate is shown in figure 1(a) and its Raman spectrum in figure 1(b). Despite the long integration time (60 min) and relatively large average NP size (110 nm), only Raman peaks belonging to the Si substrate stand out distinctly above the background. The weak spectral feature just below 200 cm^{-1}, while indeed attributable to the 195 cm^{-1} mode of VO_2, was indistinguishable from noise in the Raman spectra of arrays of smaller VO_2 NPs. In fact, it was not until 125 nm NPs were measured (not shown) that clear, though weak, VO_2 peaks emerged.

Raman scattering cross sections are typically 14–15 orders of magnitude smaller than fluorescence cross sections [18]. Raman scattering becomes increasingly less favorable for smaller NPs, since their reduced volume and elastic scattering efficiency weaken the interaction with the pump light even further. However, electromagnetic field enhancements associated with the localized surface plasmons of noble-metal nanostructures can greatly increase the interaction strength between an analyte and optical radiation. In surface-enhanced Raman scattering (SERS), the analyte, which may even consist of single molecules, is placed within a few nanometers of or in contact with the signal enhancer (usually made of Ag or Au), which can be a roughened metal substrate, granular metal film, colloidally dispersed or lithographically patterned metal NPs.

Taking advantage of lithographic technology, we fabricated hybrid Au + VO_2 nanostructures consisting of VO_2 NPs

'capped' with Au NPs (e.g. see figure 1(c)). The improvement in signal strength due to the SERS effect was spectacular: for example, the SERS spectrum in figure 1(d) shows a number of distinct VO_2 peaks, especially the two peaks at 195 and 225 cm^{-1}, even though the particle diameters in this array were smaller and the integration time much shorter than those for the bare VO_2 NPs in figure 1(a). Hybrid Au + VO_2 NPs as small as 50 nm and as large as 150 nm also produced distinguishable VO_2 peaks, but invariably of lower intensity than those from the 90 nm Au + VO_2 NPs in figure 1(c). We return to this point in section 3.3.

2. Experimental details

Arrays of Au-capped VO_2 NPs, along with an Au-covered patch of VO_2 film, were fabricated on an Si substrate as shown in figure 2: (a) electron-beam lithography (EBL: 30 kV accelerating voltage, 40 pA beam current, 50 fC dose for 90 nm NPs) in a spin-coated layer of poly(methyl-methacrylate) (PMMA: 100 nm thick), followed by chemical removal of the exposed areas; (b) pulsed-laser deposition (PLD: KrF excimer laser at $\lambda = 248$ nm, fluence $\approx$3 J cm^{-2}, V_2O_3 pressed-powder target, O_2 gas at 5 mTorr) of amorphous, sub-stoichiometric vanadium oxide ($VO_{\sim 1.7}$: 20 nm thick); (c) electron-beam evaporation of gold (Au: 15 nm thick); (d) chemical lift-off of the remaining PMMA, together with the Au and $VO_{1.7}$ overlayers; (e) thermal anneal (450 °C, O_2 gas at 250 mTorr, 30 min) of the Au + $VO_{1.7}$ structures to render the VO_2 NPs and film patch stoichiometric and crystalline [19]. The lattice spacing of the NP arrays was also varied between 75 and 250 nm in order to hold the areal coverage approximately constant.

Scanning electron micrographs (SEMs) of the Au + VO_2 film patch (figure 4(a)) and Au + VO_2 NP arrays (figures 1(c) and 4(c), (e)) reveal that the Au layer does not wet the annealed VO_2 layer very well, leading to the formation of Au islands on the film patch and 'balled-up' Au caps on the VO_2 NPs. Moreover, as particle size increases, the Au caps appear to cover less of the underlying VO_2 NPs. Another feature of the hybrid nanoparticle morphology, absent prior to the thermal anneal, is the finger-like protrusions that extend from some of the NPs or even bridge the gap between a pair of neighboring NPs (e.g. figure 4(c)). Judging from the contrast in the SEM images, most of the protrusions seem to consist of bare VO_2.

The arrays were excited using a continuous-wave laser (He–Ne: $\lambda = 633$ nm, 45 mW output power), fed through a monomode fiber into an optical microscope operated in confocal-reflection mode, then focused onto the sample with a micro-objective (60×, NA = 0.80, $1/e^2$ beam spot $\approx$ 0.5 μm). The scattered light from the Au + VO_2 NPs or film, and from the Si substrate, was collected by the same micro-objective in a backscattering geometry, filtered to reduce the elastic scattering component, and sent through a multimode fiber to a spectrometer equipped with a cooled charge-coupled-device (CCD) camera. The sample temperature was ramped by a resistive heater and maintained within $\pm$0.05 K by feedback from a temperature sensor under the heating plate.

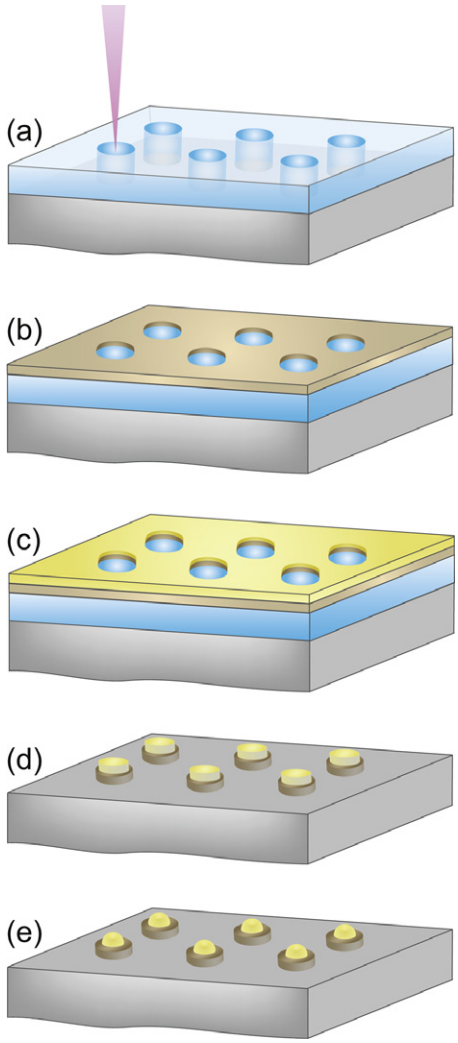

Figure 2. Fabrication of Au + VO_2 NPs (see text for details). (a) E-beam lithography and chemical development of PMMA layer on Si substrate, resulting in arrays of holes in the PMMA layer. (b) Deposition of amorphous $VO_{\sim 1.7}$ layer on patterned PMMA. (c) Deposition of Au layer on top of $VO_{1.7}$ layer. (d) Chemical lift-off of excess PMMA, Au and $VO_{1.7}$, revealing arrays of Au + $VO_{1.7}$ nanostructures. (e) Thermal anneal of Au + $VO_{1.7}$ into Au + VO_2, whereby Au NPs change morphology and $VO_{1.7}$ NPs become stoichiometric, crystalline VO_2 NPs.

Raman measurements were performed at several fixed temperatures during heating and cooling, as follows: (i) the array or film patch of interest was positioned in the laser beam spot using manual micrometers, and imaged onto another CCD camera under concurrent white-light illumination; (ii) the positioning was fine-tuned by digital adjustments to the sample stage until two designated sample features coincided with two fixed on-screen markers; (iii) the focus was visually adjusted by vertical displacement of the microscope head; (iv) an 8 min Raman spectrum was collected. The sample was then heated or cooled, and the measurement sequence repeated to map the temperature evolution of the Raman response across the structural phase transition of VO_2. We thus obtained the collective response as a function of NP size from arrays of Au-capped, nominally identical VO_2 NPs. Considering

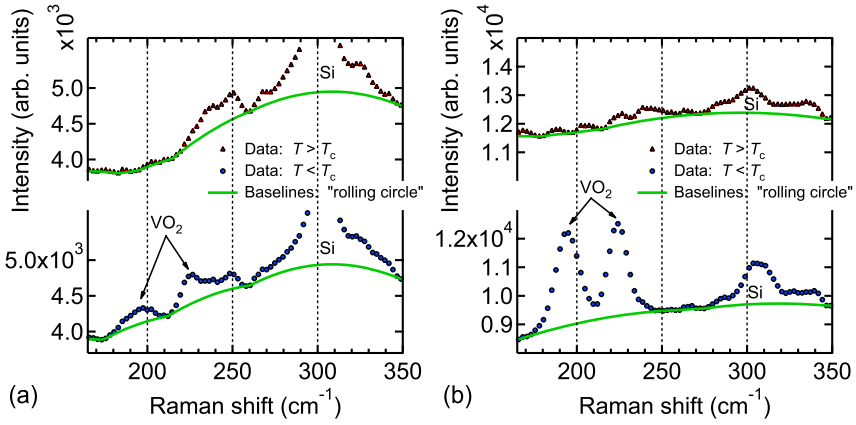

Figure 3. Representative SERS spectra from arrays of (a) 50 nm and (b) 150 nm Au + VO_2 NPs on Si, below and above their respective VO_2 transition temperatures. Solid lines denote background levels calculated using a 'rolling-circle' filter. The room-temperature (monoclinic) VO_2 peaks vanish in the high-temperature (tetragonal) phase, while features due to the Si substrate remain.

the confocal nature of these measurements, the number of simultaneously interrogated NPs varied between about 30 for the 50 nm NPs and 5 for the 150 nm NPs.

3. Results and discussion

3.1. Thermal hystereses of the Raman response

To uncover trends in the VO_2 structural transformation as a function of the amount of probed material, SERS spectra were measured from arrays of Au + VO_2 NPs of different sizes. Contrast analysis of the SEM images (e.g. figures 1(c) and 4(c) and (e)) gave the following average diameters of the VO_2 NPs: $2r \approx 50$, 60, 70, 90, 130 and 150 nm. For each of the six NP arrays and two spots on the film patch, Raman spectra were collected at ten or so temperatures during heating and cooling through the VO_2 phase transition. Figure 3 examines the region of interest from four such spectra for the smallest and largest NPs, below (at 300 K) and above (at 365 K) their transition temperatures upon heating. The vanishing of the peaks at 195 and 225 cm^{-1} marks the transition from monoclinic to tetragonal VO_2, and vice versa. The peak at 305 cm^{-1}, with a major contribution from the Si substrate, decreases in intensity above the VO_2 transition owing to the vanishing of an underlying VO_2 peak around 310 cm^{-1}. The background contribution was removed using a rolling-circle spectral filter algorithm [20]. Even after background subtraction, however, some intensity would often remain above the calculated baseline within the region of interest (175–245 cm^{-1}), mostly due to spectral features of the Si substrate, such as that near 245 cm^{-1} in figure 3(a), (top panel). Thus the integrated intensity of the VO_2 peaks differs from zero even well above T_c.

Thermal hystereses of the total above-baseline intensity between 175 and 245 cm^{-1} are presented in figure 4 for the film and for the smallest and largest NPs. The error bars denote the uncertainty in determining the total intensity according to counting statistics: $I_{total} \pm \sqrt{I_{total}}$. The significantly greater relative uncertainties in figure 4(d) stem from the much weaker Raman response of the 50 nm NPs (figure 3(a), bottom panel), as compared to the 150 nm (figure 3(b), bottom panel) or the 90 nm NPs (figure 1(d)). The lines through the hysteresis data resulted from least-squares fitting with a sigmoidal function, constrained by requiring the low- and high-temperature plateaus of the heating and cooling branches to overlap within the uncertainty of the fit. The fitting procedure provided a consistent measure of the transition temperatures for each hysteresis loop, defined here as the half-maximum points on the corresponding heating and cooling curves. Figure 5(a) summarizes those results for all six NP sizes and two separate spots on the film patch; the error bars equal $\pm 1\sigma$ as given by the fitting routine.

Taking the film as a reference, we can now look for size-dependent trends in the NP data. Most of the NP transition temperatures of the heating branch lie above the T_c of either film spot. Since we are measuring arrays of NPs, the implication is that, for example, half of the 130 nm VO_2 NPs would switch from monoclinic to tetragonal at a 7 ± 1 K higher temperature than half of the VO_2 material in the film. On the cooling branch, all the NP points lie below the corresponding T_c of the film; furthermore, the relative undercooling for the three smallest NP sizes is much more pronounced than their relative overheating. Large undercooling with respect to bulk T_c, previously observed in studies of VO_2 NPs embedded in silica [16] and arrays of VO_2 NPs on Si [15], likely arises from asymmetric shear stress [16] present on transforming from the tetragonal (high-symmetry) phase back into the monoclinic (low-symmetry) phase, although a quantitative atomic-scale explanation is still lacking. The cooling curve in figure 5(a) then suggests that, for example, half of the 50 nm VO_2 NPs would return to the monoclinic phase at a 13 ± 2 K lower temperature than half of the film volume. In VO_2 nanocrystals, such thermal 'delays' in switching phases are particularly pronounced because the availability of potent nucleation defects diminishes for smaller transforming volumes of VO_2, requiring greater deviations from bulk T_c to drive the phase transition.

3.2. Beam-induced heating and Au-VO_2 interactions

We now consider the possibility of additional heating of the VO_2 NPs by means of light-energy dissipation in the Au caps.

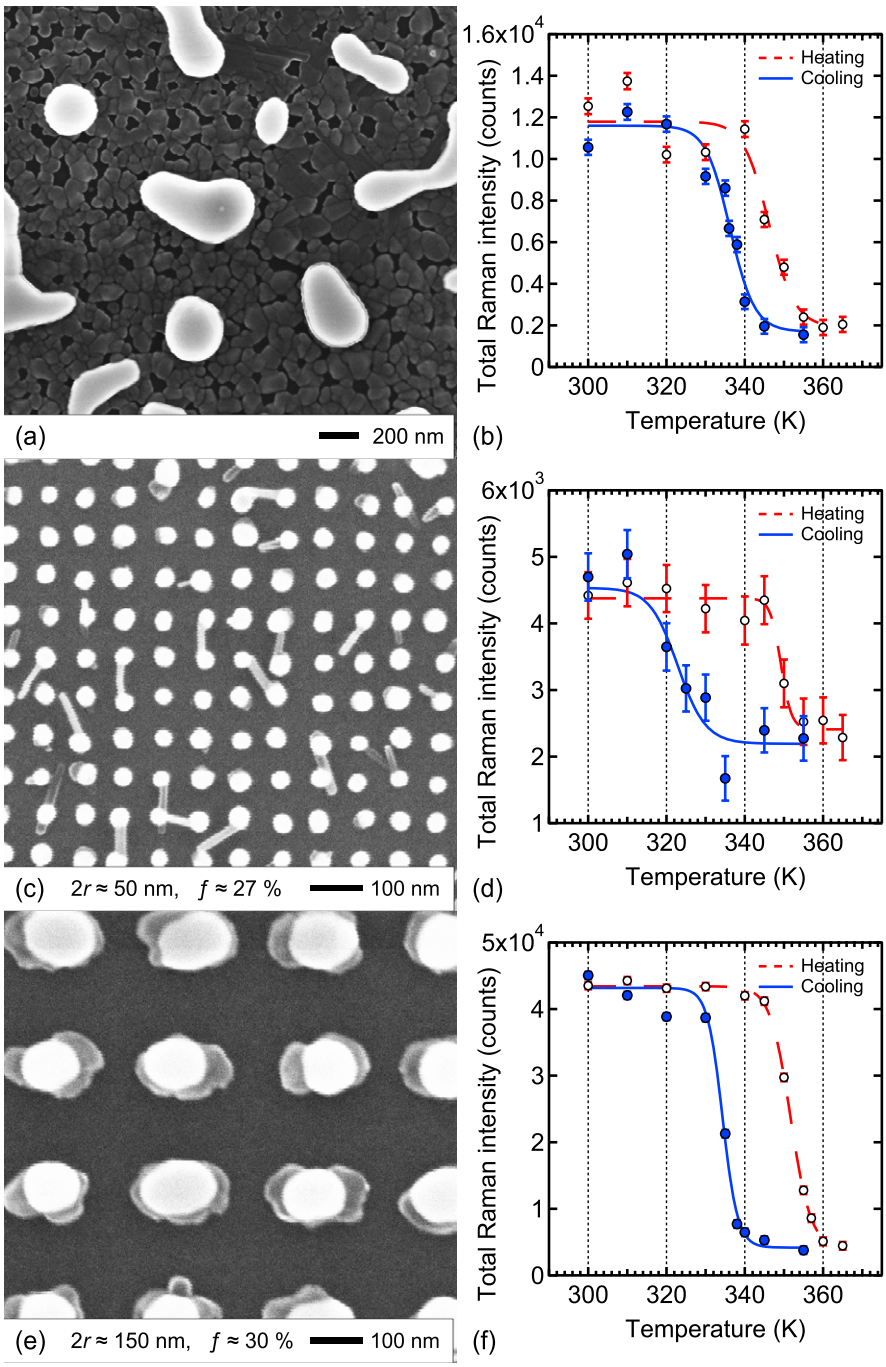

Figure 4. SEM images of (a) Au islands on VO_2 film on Si substrate and ((c), (e)) arrays of Au-capped VO_2 NPs ($2r \equiv VO_2$ NP diameter; $f \equiv VO_2$ areal coverage). Thermal hystereses of SERS intensity of VO_2 peaks, summed between 175 and 245 cm^{-1} after 'rolling-circle' background subtraction (see figure 3), for (b) Au + VO_2 film and Au + VO_2 NPs of (d) $2r = 50$ nm and (f) $2r = 150$ nm. Lines are fits to the data points using an empirical sigmoidal function.

For example, optical illumination of Au NPs embedded in ice generates localized heat and even melts the surrounding matrix, especially for photon energies close to the particle–plasmon resonance [21]. The maximum increase in local temperature due to plasmonic heating is expected to occur at the surface of the Au particle and scale with the square of its radius [21, 22]. It is then conceivable that the VO_2 transition temperatures obtained here may have been biased by localized heating of the Au NPs by the pump laser. Such an effect would manifest itself as an artificial decrease in the observed T_c *in either direction*: less external energy would need to be added for sample heating but more dissipated through cooling. However, neither the heating nor the cooling branches in figure 5(a) shows a progressive lowering of T_c as the VO_2 NPs (hence, the Au caps) increase in size. Therefore, heating of the VO_2 NPs by the Au caps, albeit possible in principle, is ruled out by the present data.

The width of the thermal hysteresis is a measure of the intrinsic size dependence of the phase transition that remains unaffected by a constant temperature bias. A contiguous VO_2

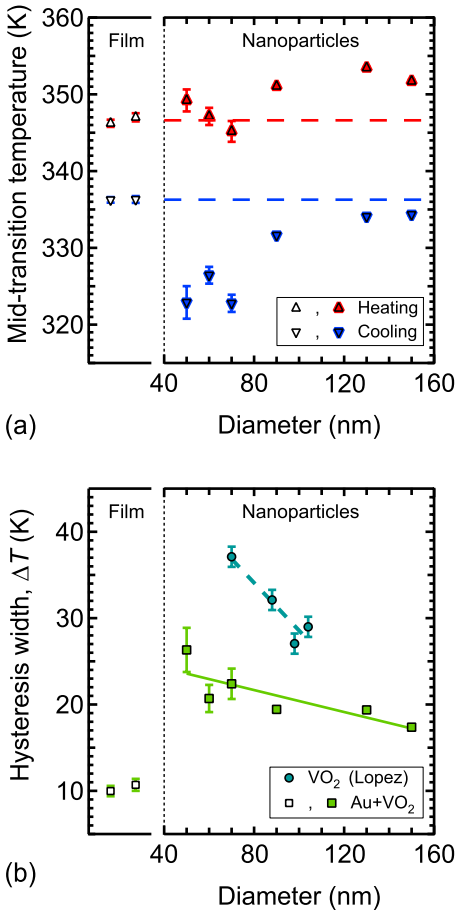

Figure 5. (a) Transition half-maximum points of heating and cooling branches of SERS hystereses (obtained from sigmoidal fits in figure 4) for two different spots on the Au + VO_2 film (left panel: open triangles; right panel: dashed lines) and for all six NP sizes (right panel: filled triangles). (b) Comparison between hysteresis widths from SERS measurements on Au + VO_2 film (left panel: open squares) and NPs (right panel: filled squares) on Si (this work) and hysteresis widths from light-scattering measurements on bare VO_2 NPs (right panel: filled circles) on Si (after Lopez *et al* [15]). Also shown are least-squares linear fits through each dataset.

film has a relatively narrow hysteresis (typically, $\Delta T = 10$–15 K) because many potent sites for heterogeneous nucleation reside in its large accessible volume, so that relatively small excursions in temperature can initiate the phase transition. In contrast, smaller amounts of VO_2 material generally require substantial overheating and undercooling (i.e. excess driving forces) to change from the monoclinic to the tetragonal phase and back again, widening the thermal hysteresis. Figure 5(b), where the square points are obtained directly from figure 5(a), corroborates this trend: $\Delta T_{\text{film}} = 10.5 \pm 0.5$ K, whereas $\Delta T_{50\text{ nm NPs}} = 26.5 \pm 2.5$ K. Moreover, the hysteresis width shrinks with increasing NP size (e.g. $\Delta T_{150\text{ nm NPs}} = 17.5 \pm 0.5$ K), since an increase in probed volume per particle should result in a greater average probability that any given NP contains at least one site capable of heterogeneously nucleating the phase transition [16].

Also shown in figure 5(b) (circles) are the hysteresis widths for arrays of VO_2 NPs from the light-scattering experiments of Lopez *et al* [15]. In comparison with the present study (figure 5(b), squares), the bare-VO_2 NPs exhibit a larger magnitude and steeper slope of ΔT as a function of NP size. Such a difference may be intrinsic or associated with the specific experimental configuration. It may be tempting to attribute these differences to the two different components of the VO_2 transition, electronic (via elastic light scattering) versus structural (via SERS). However, a number of experimental factors must be taken into account before such a hypothesis can be confirmed. The Au caps on the VO_2 NPs likely affect the underlying VO_2 material in two distinct ways. On the one hand, the Au caps clearly enhance the weak Raman signal from the VO_2 NPs, but, on the other, the caps may either introduce new potent defects at the Au–VO_2 interface (especially during the thermal anneal) or 'passivate' such nucleation sites as would have existed on the top surfaces of bare VO_2 NPs (i.e. without Au caps). The finger-like protrusions pointed out in section 2 suggest that the presence of the Au layer does impact the growth of the VO_2 NPs; in fact, doping VO_2 films with Au is known to reduce the width and steepness of the hysteresis in infrared transmission [23]. Adding extrinsic defect sites to those ones mandated by the statistics of heterogeneous nucleation [16] would narrow the hysteresis width, thus obscuring its size dependence. Nevertheless, the present study supports the notion that the size effect in the VO_2 transition is a statistical manifestation of a more fundamental factor: the presence or absence of nucleating sites active at a given temperature.

3.3. Size dependence of the SERS intensity

We mentioned in section 1.2 that the 90 nm Au + VO_2 NPs generated the strongest Raman signals. Indeed, a distinct size effect is evident from figure 6(a), which compares the experimental maxima of the total Raman intensity under the two VO_2 peaks for all six NP sizes and the film patch; the particle sizes here refer to the diameters of the Au caps, which image analysis determined to be approximately 5–40 nm smaller than the underlying VO_2 NPs (e.g. see figure 4(e)). The strongest SERS signal therefore came from the 90 nm VO_2 NPs with the 75 nm Au caps on top.

The main contribution to signal enhancement in SERS, the electromagnetic effect, scales roughly with the fourth power of the electric-field enhancement, since the vibrational frequencies of the analyte are small compared with the plasmon bandwidth of the metal. The local fields at both the excitation frequency of the incident radiation and the Stokes-shifted frequency of the induced-dipole radiation are therefore enhanced [18, 24]. Since both of these enhancement factors originate from the interaction of optical radiation with metal nanostructures, the scattering efficiency of a field enhancer determines the magnitude of SERS enhancement.

Figure 6(b) shows an analytical calculation of the scattering efficiency as a function of size for a spherical Au particle immersed in a composite host, based on Mie scattering [25] modified to account for absorption in the host medium [26]. The complex permittivity of the host comprises weighted contributions of VO_2 and air; the permittivity of Au

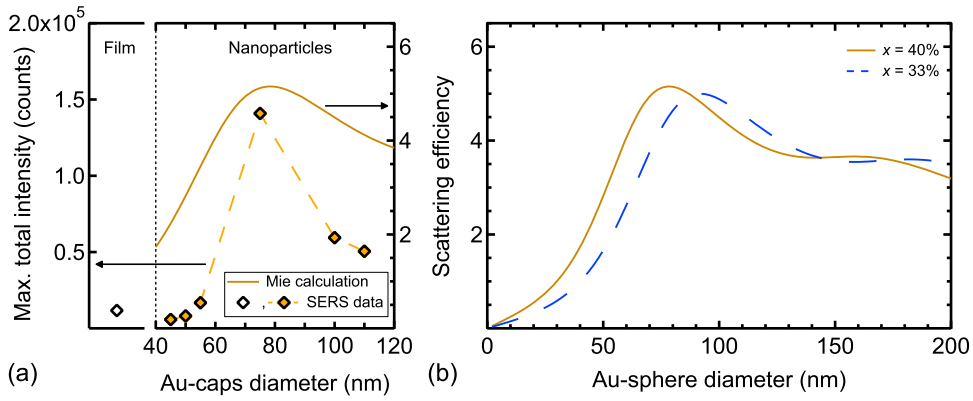

Figure 6. (a) Total SERS intensity at 300 K (from hysteresis curves in figure 4) as a function of size of Au caps (right panel); the dashed line is only a guide for the eyes; the solid line is the same Mie calculation as the solid line in (b); the value for the Au + VO_2 film is also shown (left panel). (b) Mie-theory calculations (modified for absorbing host medium) of scattering efficiency as a function of particle diameter for Au sphere in composite host medium consisting of $\frac{2}{5}$ ($x = 40\%$) semiconducting-phase VO_2 and $\frac{3}{5}$ air (solid line) or $\frac{1}{3}$ ($x = 33\%$) semiconducting-phase VO_2 and $\frac{2}{3}$ air (dashed line). Incident light: $\lambda = 633$ nm. The highest efficiency for $x = 40\%$ occurs at $2r_{Au} = 75$ nm, in agreement with the Au-cap size yielding the largest experimental SERS intensity in (a).

was obtained from [27] and that of VO_2 from [28]. The specific choice of 33% VO_2 and 67% air (figure 6(b), dashed line) is based on the geometry of a hemisphere on a flat surface: $\frac{1}{3}$ of the cap's surface area lies in contact with VO_2 and $\frac{2}{3}$ with air. The predicted maximum scattering efficiency of such Au NPs peaks at $2r_{Au} = 90$ nm, relatively close to $2r_{Au} = 75$ nm, which is the highest experimental datum in figure 6(a). For even better agreement, the calculation needs only a small adjustment—40% instead of 33% VO_2 contribution—to yield a maximum in the Au-NP scattering efficiency at $2r_{Au} = 75$ nm (figure 6(b), solid line), also overlaid on the experimental data in (a)). This scenario of 40% VO_2 and 60% air corresponds to a contact angle of less than 90° between the Au caps and the underlying VO_2 layer. Considering the simplifications employed in the calculation, the semi-quantitative correlation in figure 6(a) between the size dependence of the SERS signal and the calculated scattering efficiency supports the main points of this analysis.

4. Summary and outlook

We have reported the first experimental application of surface-enhanced Raman scattering (SERS) to the study of the phase transition of VO_2. The electromagnetic enhancement of the VO_2 Raman signal, caused by the plasmonic properties of Au particles, was instrumental to this experiment, since no Raman signal could be obtained from bare VO_2 NPs of sizes less than 125 nm. The structures fabricated on an Si substrate were: (i) VO_2 NPs of different diameters (50–150 nm), arranged in regular arrays of nominally identical NPs, with each VO_2 NP capped with a somewhat smaller Au particle (45–110 nm) and (ii) a contiguous VO_2 film covered with disconnected Au islands. On comparing NPs to film, we found that the NPs required a larger 'driving force' to complete the phase transformation, as shown by the wider thermal hysteresis. We also observed the trend expected from a model of heterogeneous nucleation of the VO_2 transition [16], namely that the 50 nm VO_2 NPs produced the widest thermal hysteresis (figure 5(b)), since the smallest VO_2 volume should have the least statistical likelihood of harboring a potent site for nucleating the phase transition.

The size effect proved less pronounced for the Au + VO_2 NPs studied here than for the bare VO_2 NPs in the light-scattering experiment [15]. We offer a heuristic explanation: during high-temperature annealing, the Au metal may contribute extrinsic defects to the VO_2 NPs, thus masking the correlation between size (scarcity of nucleation sites) and hysteresis width (driving force needed to activate latent nucleation sites). On the other hand, the Au caps may modify the VO_2 surface in such a way as to disable potential nucleation sites, and thus aid in widening the thermal hysteresis of the structural transformation, which may indeed have a different size dependence from the electronic transformation.

Our study also shows that the measured SERS intensity scales according to NP size, peaking for the 75 nm Au + 90 nm VO_2 NPs (figure 6(a)), in good agreement with Mie-theory predictions for the scattering efficiency of an Au sphere surrounded by a mixture of VO_2 and air (figure 6(b)).

The experiment described here can improve the throughput of confocal Raman mapping measurements of individual VO_2 NPs [17], with the aim of constructing many single-particle hystereses to look for statistical links between hysteresis width and VO_2 NP morphology.

Acknowledgments

We thank A B Hmelo for assistance with the e-beam lithography and Nicki Davis for creating figure 2. This work was supported by the United States Department of Energy, Office of Science (DE-FG02-01ER45916).

References

[1] Morin F J 1959 *Phys. Rev. Lett.* **3** 34–6
[2] Goodenough J B 1971 *J. Solid State Chem.* **3** 490–500

[3] Imada M, Fujimori A and Tokura Y 1998 *Rev. Mod. Phys.* **70** 1039–263
[4] Zylbersztejn A and Mott N F 1975 *Phys. Rev.* B **11** 4383–95
[5] Paquet D and Hugon P L 1980 *Phys. Rev.* B **22** 5284–301
[6] Wentzcovitch R M, Schulz W W and Allen P B 1994 *Phys. Rev. Lett.* **72** 3389–92
[7] Rice T M, Launois H and Pouget J P 1994 *Phys. Rev. Lett.* **73** 3042
[8] Wentzcovitch R M, Schulz W W and Allen P B 1994 *Phys. Rev. Lett.* **73** 3043
[9] Cavalleri A, Dekorsy T, Chong H H W, Kieffer J C and Schoenlein R W 2004 *Phys. Rev.* B **70** 161102
[10] Biermann S, Poteryaev A, Lichtenstein A I and Georges A 2005 *Phys. Rev. Lett.* **94** 026404
[11] Kim H T, Lee Y W, Kim B J, Chae B G, Yun S J, Kang K Y, Han K J, Yee K J and Lim Y S 2006 *Phys. Rev. Lett.* **97** 266401
[12] Qazilbash M M *et al* 2007 *Science* **318** 1750–3
[13] Kübler C, Ehrke H, Huber R, Lopez R, Halabica A, Haglund R F Jr and Leitenstorfer A 2007 *Phys. Rev. Lett.* **99** 116401
[14] Baum P, Yang D S and Zewail A H 2007 *Science* **318** 788–92
[15] Lopez R, Feldman L C and Haglund R F Jr 2004 *Phys. Rev. Lett.* **93** 177403
[16] Lopez R, Haynes T E, Boatner L A, Feldman L C and Haglund R F Jr 2002 *Phys. Rev.* B **65** 224113
[17] Donev E U, Lopez R, Feldman L C and Haglund R F Jr 2009 *Nano Lett.* **9** 702–6
[18] Novotny L and Hecht B 2006 *Principles of Nano-Optics* (Cambridge: Cambridge University Press)
[19] Suh J Y, Lopez R, Feldman L C and Haglund R F Jr 2004 *J. Appl. Phys.* **96** 1209–13
[20] Brandt N N, Brovko O O, Chikishev A Y and Paraschuk O D 2006 *Appl. Spectrosc.* **60** 288–93
[21] Richardson H H, Hickman Z N, Govorov A O, Thomas A C, Zhang W and Kordesch M E 2006 *Nano Lett.* **6** 783–8
[22] Govorov A O, Zhang W, Skeini T, Richardson H, Lee J and Kotov N A 2006 *Nanoscale Res. Lett.* **1** 84–90
[23] Cavanna E, Segaud J P and Livage J 1999 *Mater. Res. Bull.* **34** 167–77
[24] Maier S A and Atwater H A 2005 *J. Appl. Phys.* **98** 011101
[25] van de Hulst H C 1981 *Light Scattering by Small Particles* (New York: Dover)
[26] Sudiarta I W and Chylek P 2001 *J. Opt. Soc. Am.* A **18** 1275–8
[27] Palik E D 1985 *Handbook of Optical Constants of Solids* (*Academic Press Handbook Series*) (Orlando: Academic)
[28] Verleur H W, Barker A S and Berglund C N 1968 *Phys. Rev.* **172** 788–98